Editors' Suggestion

Optical Detection of Long Electron Spin Transport Lengths in a Monolayer Semiconductor

L. Ren (任磊),[1,*] L. Lombez,[1,*] C. Robert,[1,*,†] D. Beret,[1] D. Lagarde,[1] B. Urbaszek,[1] P. Renucci,[1] T. Taniguchi,[2] K. Watanabe,[3] S. A. Crooker,[4] and X. Marie[1,‡]

[1]*Université de Toulouse, INSA-CNRS-UPS, LPCNO, 135 Av. Rangueil, 31077 Toulouse, France*
[2]*International Center for Materials Nanoarchitectonics, National Institute for Materials Science, 1-1 Namiki, Tsukuba 305-00044, Japan*
[3]*Research Center for Functional Materials, National Institute for Materials Science, 1-1 Namiki, Tsukuba 305-00044, Japan*
[4]*National High Magnetic Field Laboratory, Los Alamos National Laboratory, Los Alamos, New Mexico 87545, USA*

(Received 27 January 2022; accepted 18 May 2022; published 5 July 2022)

Using a spatially resolved optical pump-probe experiment, we measure the lateral transport of spin-valley polarized electrons over very long distances (tens of micrometers) in a single WSe_2 monolayer. By locally pumping the Fermi sea of 2D electrons to a high degree of spin-valley polarization (up to 75%) using circularly polarized light, the lateral diffusion of the electron polarization can be mapped out via the photoluminescence induced by a spatially separated and linearly polarized probe laser. Up to 25% spin-valley polarization is observed at pump-probe separations up to 20 μm. Characteristic spin-valley diffusion lengths of 18 ± 3 μm are revealed at low temperatures. The dependence on temperature, pump helicity, pump intensity, and electron density highlight the key roles played by spin relaxation time and pumping efficiency on polarized electron transport in monolayer semiconductors possessing spin-valley locking.

DOI: 10.1103/PhysRevLett.129.027402

Atomically thin transition metal dichalcogenide (TMD) semiconductors such as MoS_2 have sparked a renewed interest in exploiting both spin and valley degrees of freedom, owing to the remarkable spin-valley locking effects that originate from their lack of inversion symmetry and strong spin-orbit coupling [1–4]. This dictates that the spin and valley degrees of freedom for carriers in the band extrema (electron in the bottom conduction band or holes in the top valence band) are mutually protected; i.e., relaxation requires both a change of valley (for instance, with a momentum-conserving phonon) and also a spin flip. (In the following and for simplicity we will mainly use the term "spin" instead of spin-valley knowing that the two degrees of freedom are coupled.) An important consequence is that electron or hole spin relaxation times can reach very large values—in the microsecond range [5–7]. One can expect that this spin-valley locking will also have a strong impact on the lateral transport of electron spin polarization [8]. However, very little is known about the spatial dependence of free carrier spin polarization in these TMD monolayers (ML) despite its crucial relevance for spin(valley)tronics applications using 2D materials [9–11]. Spatial mapping of lateral spin transport in these 2D layers is also important from the point of view of fundamental physics, as it should reveal critical information about possible magnetic phase transitions and valley-polarized collective states that have been theoretically predicted in electron- or hole-doped TMD ML [12–14].

Spatial mapping studies of spin polarization are scarce since (i) in transport experiments, the fabrication of four-terminal nonlocal geometry devices is very challenging with a single TMD ML [15,16] and (ii) in optical measurements, the properties are usually dominated by robust exciton complexes that are characterized by picosecond lifetimes and very limited diffusion lengths, i.e., typically ~ 1 μm at low temperature [17–25]. Small spin diffusion lengths of holes L_s less than 0.1 μm were estimated from valley Hall effect measurements in a WSe_2 ML [26], whereas electron spin transport investigations in few-layer MoS_2 using a two-terminal spin-valve configuration geometry yielded $L_s \sim 0.4$ μm [27]. The spin-valley diffusion properties have also been investigated in WS_2-WSe_2 bilayer heterostructure where the diffusion length is controlled by both inter-layer excitons and resident holes [28].

Here, we locally polarize the Fermi sea of resident electrons in an n-doped WSe_2 ML with a *circularly* polarized pump laser, and study how the imbalance between spin-up (K' valley) and spin-down (K valley) electrons evolves in space by using a weak *linearly* polarized probe laser to induce photoluminescence (PL) at a tunable distance d from the pump spot. The circular

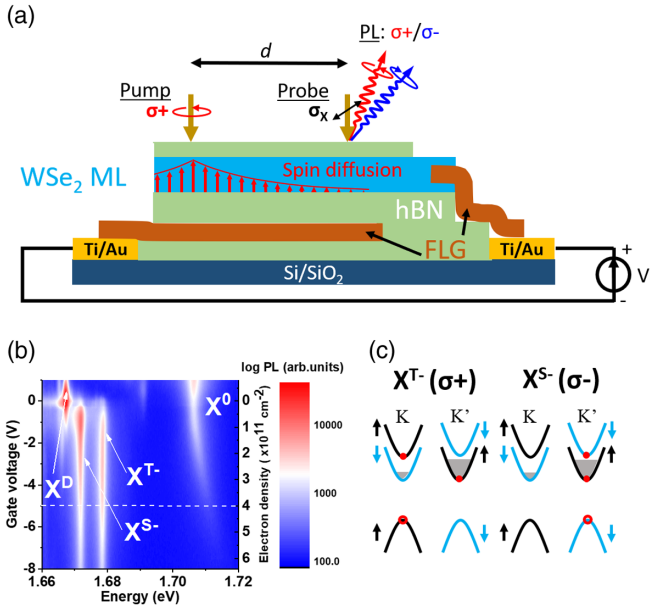

FIG. 1. (a) Sketch of the charge tunable WSe_2 ML (not to scale). Two laser spots (pump and probe) separated by a distance d, are focused on the sample. The pump is circularly polarized ($\sigma+$) and dynamically polarizes the resident electrons in the K' valley with spin up. This spin-valley polarization diffuses over long distances (sketched by the vertical red arrows representing the average electron spin along the direction perpendicular to the ML) and is detected by a linearly polarized (σ_X) probe. The circular polarization of the probe-induced X^{S-} and X^{T-} PL provides a quantitative measurement of the polarization of the 2D electron sea at the location of the probe spot. (b) Characterizing the PL from the sample vs gate voltage (i.e., electron doping density) for the case of a single excitation laser. The horizontal dashed line indicates the doping region where the experiment is conducted. (c) Three-particle configurations of triplet (X^{T-}) and singlet (X^{S-}) trions, when resident electrons are polarized in the K' valley. X^{T-} (X^{S-}) mainly emits $\sigma+$ ($\sigma-$) PL.

polarization of the induced trion PL reveals the spin polarization of the resident electrons at the probe's location. We demonstrate that the polarization of resident electrons can propagate over very large distances; we detect polarizations as large as 25% at a pump-probe separation of $d = 20$ μm. The spatial decay of the electron polarization yields typical spin diffusion length up to $L_s = 18$ μm at $T = 7$ K. Finally, we show that the spin-valley pumping efficiency decreases as the temperature increases, as a consequence of the strongly temperature-dependent spin-valley relaxation time.

Figure 1(a) presents a schematic of the pump-probe PL experiment performed on a high-quality charge-adjustable WSe_2 ML encapsulated in hBN [29]. Continuous wave He-Ne laser beams ($\lambda = 632.8$ nm) are used for both pump and probe. Using the same high numerical aperture objective, the two beams are focused on the sample at two different positions separated by a distance d. Spots sizes are ~ 1 μm diameter. The pump beam is right circularly polarized ($\sigma+$), whereas the probe beam is linearly polarized (σ_x). We detect both right ($\sigma+$) and left ($\sigma-$) circularly polarized luminescence triggered by the probe beam, as a function of the pump-probe separation d. Details of the sample fabrication and the experimental setup are given in the Supplemental Material [30] S1, S2, and S3, which includes Refs [31–34].

We first show in Fig. 1(b) the characteristic PL response of the device as a function of bias voltage (i.e., electron density) in response to a single excitation laser. In agreement with many previous reports, the PL spectra in the high energy range are dominated by the recombination of the bright (X^0) the dark (X^D) neutral exciton and the well identified intravalley (singlet) X^{S-} and intervalley (triplet) X^{T-} negatively charged excitons which are composed of two electrons and one hole [see Fig. 1(c)] [35–37]. In the moderate doping density regime investigated here (a few 10^{11} cm^{-2}), the resident electrons only populate the lower conduction bands in both the K and K' valleys. Note that in this small doping regime the three-particle picture (i.e., trion) and the Fermi-polaron description are both relevant [10,38].

Importantly the degree of circular polarization of the X^{T-} and X^{S-} PL can serve as a quantitative probe of the spin-valley polarization of the resident electrons, as demonstrated in Ref. [39] and as summarized below. Assuming that the trions are formed through the binding of photogenerated bright excitons with a resident electron (i.e., a bimolecular formation process [40]), the circular polarization of the triplet $P_c(X^{T-})$ and singlet $P_c(X^{S-})$ are simply related to the spin polarization of the resident electrons $P_e = [(n_e^{\uparrow K'} - n_e^{\downarrow K})/(n_e^{\uparrow K'} + n_e^{\downarrow K})]$ [where $n_e^{\uparrow K'}$ and $n_e^{\downarrow K}$ are the populations of resident electrons with spin-up (K' valley) and spin-down (K valley)] and the polarization of the photogenerated excitons $P_0 = [(N_0^K - N_0^{K'})/(N_0^K + N_0^{K'})]$ (where N_0^K and $N_0^{K'}$ are the populations of photogenerated bright excitons with carriers in the K and K' valleys):

$$\text{Triplet } P_c(X^{T-}) = \frac{P_0 + P_e}{1 + P_0 P_e}. \quad (1)$$

$$\text{Singlet } P_c(X^{S-}) = \frac{P_0 - P_e}{1 - P_0 P_e}. \quad (2)$$

By measuring both $P_c(X^{T-})$ and $P_c(X^{S-})$ we can thus easily quantify the polarization of the resident electrons P_e.

We first characterize in Fig. 2(a) the PL spectra emitted following a circularly polarized ($\sigma+$) laser excitation (power $= 5$ μW and electron doping density $= 4 \times 10^{11}$ cm^{-2}). The circular polarization of the triplet trion X^{T-} PL reaches very large positive values, while it is negative for the singlet trion X^{S-} PL. This is a direct consequence of a spin-valley pumping mechanism that

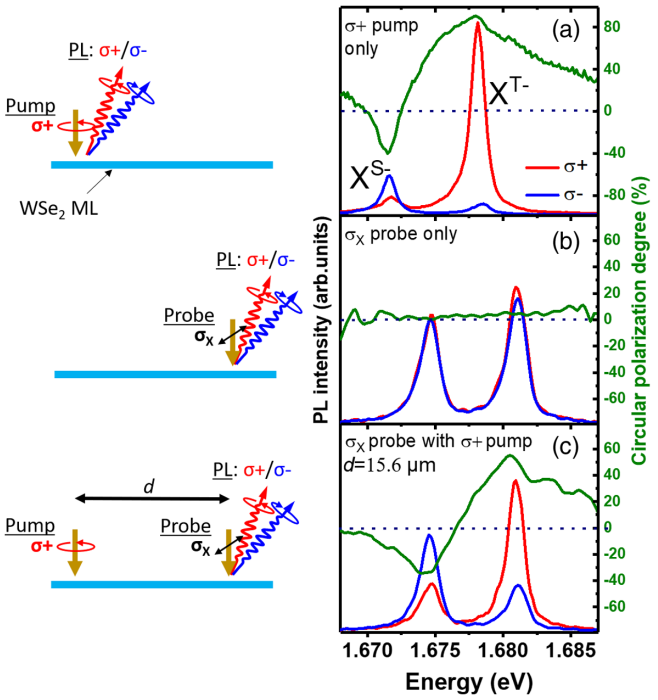

FIG. 2. Right ($\sigma+$) and left ($\sigma-$) circularly polarized PL spectra and corresponding circular polarization degree, in response to (a) the $\sigma+$ pump only, (b) the linear σ_X probe only and (c) the σ_X probe in the presence of a $\sigma+$ pump separated by distance $d = 15.6$ μm. The strong circular polarization of the trion PL demonstrates that the resident electrons are strongly spin-valley polarized at the position of the probe laser. $T = 5$ K.

dynamically polarizes the resident electrons in the K' valley with spin-up [39]. Note that the efficiency of the spin-valley pumping mechanism depends on both excitation power and doping density. The electron density chosen here maximizes the electron spin polarization while keeping a sufficiently intense trion PL [39]. Using the values of $P_c(X^{T-})$ and $P_c(X^{S-})$, we find that the polarization of resident electrons induced by the laser attains values as large as $P_e = 76\%$ (i.e., the resident electrons mainly populate the lower spin-up conduction band in the K' valley) while the polarization of the photogenerated excitons P_0 is 51%.

We then show, in Fig. 2(b), the PL spectra emitted following a weak linearly polarized (σ_X) laser excitation (power = 200 nW). As expected, there is no circular polarization of X^{T-} or X^{S-} PL because $P_0 = 0$ (linear excitation) and $P_e = 0$ (no spin-valley pumping mechanism for linear excitation).

Figure 2(c) shows the first key result of our work. It presents the PL spectra induced by the weak σ_X laser (probe), but now in the presence of the $\sigma+$ laser (pump) that is separated by a distance $d = 15.6$ μm (see the Supplemental Material [30] S3 and S4 for a detailed description of the experimental protocol). Remarkably, now we observe a very large circular polarization for both trions ($\sim +50\%$ for X^{T-} and $\sim -40\%$ for X^{S-}). Because $P_0 = 0$ for the probe (linear excitation), this result directly reveals the polarization of the resident electrons at the location of the probe [i.e., $P_c(X^{T-}) = P_e$ and $P_c(X^{S-}) = -P_e$; see Eqs. (1) and (2)]. Because the linearly polarized probe itself does not polarize the resident electrons (as shown above), this demonstrates that the spin polarization of the resident electrons induced by the pump propagates in the 2D layer plane and can be detected by measuring the circular polarization of the trion PL below the probe. A key advantage of this PL-based pump-probe experiment in comparison to well-known and powerful Kerr or Faraday rotation spin imaging methods [41,42] is that it allows to quantify, in absolute terms, the spin polarization of the electron Fermi sea. We show in the Supplemental Material [30] S5 and S6 the dependence of the signal on both pump and probe power as well as the dependence with the doping density.

Figure 3(a) presents the main result of this work. It displays the dependence of the probe PL circular polarization of both trions as a function of the pump-probe separation d. Additional details are given in the Supplemental Material [30] S9 that includes Ref [43]. A spatial decay of the spin polarization of resident electrons is clearly evidenced, but the resident electron polarization induced by the pump can propagate on length scales larger than 20 μm. We find that the spin polarization decays approximately exponentially with a spin diffusion length of $L_s = 18 \pm 3$ μm. This is among the longest spin diffusion lengths reported in semiconductors, despite a modest carrier mobility [44–46]. It is ten times larger than L_s measured in silicon or p-type GaAs at low temperature, and is similar to the spin diffusion length measured in n-doped GaAs bulk [42,47–49] or quantum wells [50–52]. Remarkably, the spin diffusion length we measure here for a WSe_2 ML is very similar to the one determined in graphene monolayers, which are usually characterized by a much larger electron mobility and lower spin-orbit coupling. Using 'nonlocal' spin valve geometries in graphene, spin diffusion lengths of 2 μm were measured and record values of $L_s = 30$ μm were more recently reported [53,54]. This underlines the key role played by the spin-valley locking effect in TMD ML on carrier spin propagation. Note that the measured spin diffusion length of 18 μm is consistent with electron spin-valley relaxation time and electron mobilities recently measured in very comparable n-doped WSe_2 ML devices. In a simplified picture based on Einstein relations, we can infer a calculated spin diffusion length of $L_s = \sqrt{D_s \tau_s} \sim 10\,\mu$m, using: (i) the electron mobility μ_e recently measured in hBN encapsulated TMD MLs—typically 3000 $cm^2/(V.s)$ [44–46] and assuming that the spin diffusion coefficient is equal to the charge diffusion coefficient ($D_s = D_c \approx \mu_e kT/e$) [52,54]; (ii) the spin-valley relaxation time

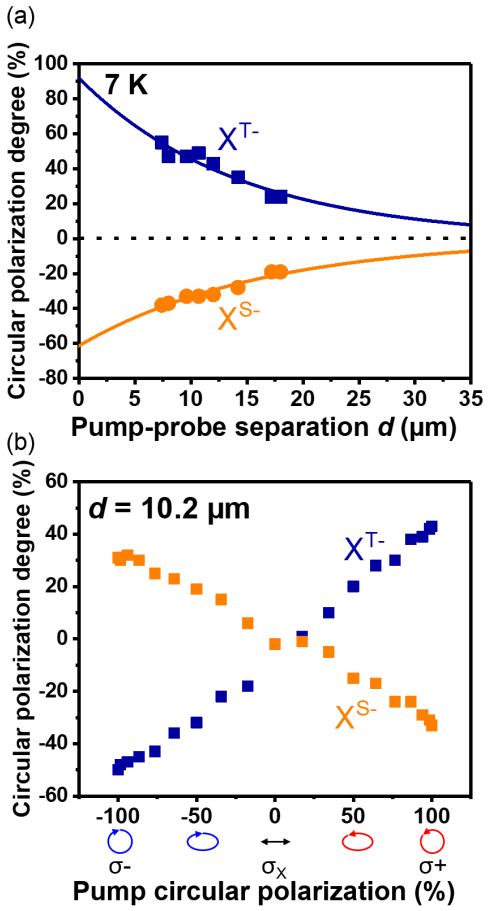

FIG. 3. (a) Circular polarization degree of the X^{T-} and X^{S-} trion PL, as a function of the pump-probe separation d. The solid lines are exponential fits. (b) Circular polarization degree of X^{T-} and X^{S-} trion PL, at a fixed pump-probe separation, versus the pump helicity. $T = 7$ K.

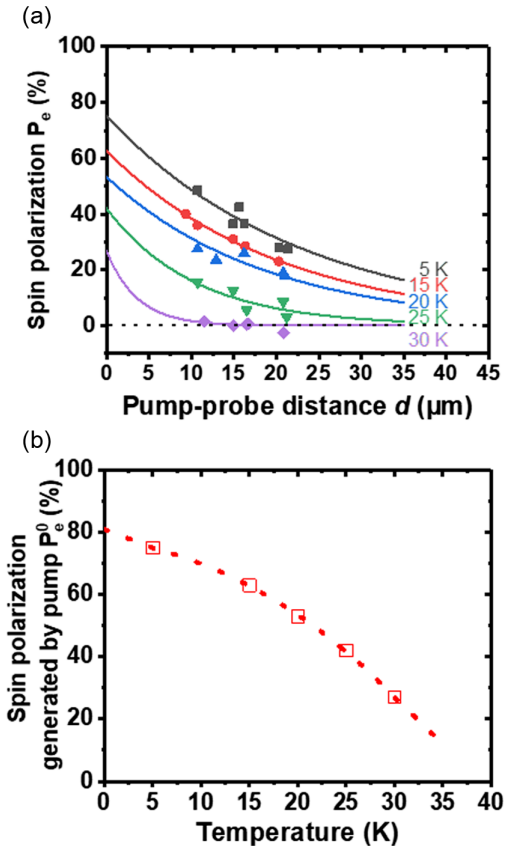

FIG. 4. (a) Temperature dependence of the spin polarization of the resident electrons (P_e) at the probe location, versus pump-probe separation d. (b) Spin polarization generated below the pump spot (P_e^0) as a function of temperature, as extracted from the measurement of the circular polarization of X^{T-} and X^{S-} shown in the Supplemental Material [30] S8. The red dotted line is a guide for the eye. These values of P_e^0 are used to fit the results of panel (a) with monoexponential decays $P_e(d) = P_e^0 \exp(-d/L_S)$ that are shown by the solid lines.

obtained from time-resolved Kerr rotation (~1 μs for a doping density of about 4×10^{11} cm^{-2}) shown in the Supplemental Material [30] S7.

Next, we demonstrate that the electron spin polarization detected at the probe location smoothly tracks the helicity of the pump beam as expected for spin diffusion process. Figure 3(b) presents the circular polarization degree of X^{T-} and X^{S-} at the probe spot when the pump spot is continuously tuned from purely circular $\sigma+$ to purely circular $\sigma-$ through elliptical and linear polarizations. As expected we observe a change of sign of PL circular polarization when the helicity of the pump is reversed, and a near-linear dependence of the electron spin polarization on the circular polarization degree of the pump excitation.

Finally, we investigate the temperature dependence of the lateral transport of electron spin in the WSe_2 ML. Figure 4(a) shows the spin polarization of the resident electrons P_e as a function of the pump-probe separation, and at various temperatures. Because slightly different values of P_e can be inferred from the polarization of X^{T-} and X^{S-} (see Fig. 3), we plot here an average between the two values ($P_e = \{[P_c(X^{T-}) - P_c(X^{S-})]/2\}$). While electron spin transport can be clearly observed up to a temperature of 25 K, the amplitude of the spin polarization decreases compared to the measurements at $T = 5$ K. For temperatures larger than 25 K, no spin polarization can be observed at a distance larger than 10 μm. It turns out that the main origin of this drop of the non-local spin polarization is the decrease of the efficiency of the spin pumping itself, i.e., the generation of spin polarized resident electrons by the pump. Figure 4(b) displays temperature dependence of the resident electron spin polarization obtained from the measured X^{T-} and X^{S-} trion PL circular polarizations induced by the pump and detected at the pump location [39] (same experiment as in Figure 2(a), raw data are shown in the Supplemental Material [30] S8). We observe that the dynamical polarization of the resident electrons decreases drastically between 5 and 30 K. This is a consequence of the decrease of the spin-valley pumping

efficiency itself, due to the decrease of the spin-valley relaxation time which drops by a factor ∼10 in this temperature range, as measured recently by time-resolved Kerr rotation experiments on a similar gated and hBN-encapsulated WSe_2 ML [6].

We note that our spatially resolved studies are consistent with lateral diffusion of spin polarized electrons in the WSe_2 monolayer, and do not show evidence of a spontaneous magnetic ordering in the spin-polarized electron gas, as was theoretically predicted to occur in TMD MLs as a consequence of strong exchange interactions [12–14,55]. Specifically, the measured non-local electron polarization varies smoothly with changes in pump intensity, pump helicity, and temperature, and does not show any abrupt discontinuities or saturation or hysteresis that would indicate a transition to an ordered ferromagnetic phase. Moreover, the approximately exponential spatial decay of the polarization signal is in line with expectations of a spin diffusion process, and does not show any sudden variations that might be expected from the formation of ferromagnetically-ordered domains.

In conclusion we have investigated the spin-valley diffusion transport of free electrons in a WSe_2 ML. In contrast to previous investigations in TMD MLs where the diffusion properties were dominated by short-lived exciton complexes, the efficient spin-valley pumping of resident electrons allows us to evidence transport of spin-valley information over very long distances, with a typical diffusion length of 18 μm. This is a consequence of the long spin-valley relaxation time induced by the unique spin-valley locking effect in this atomically thin crystal. To separate the effects of diffusion and relaxation, spin grating experiments could be performed in the future to measure accurately the spin diffusion coefficient independently from the charge diffusion coefficient [50,51]. We also anticipate that improvements in the charge mobility of carriers in higher quality material [56] may result in longer spin diffusion length. Spatially extended hole spin diffusion is also expected in these TMD monolayers, given similarly long spin-valley lifetimes and even stronger spin-valley locking due to the huge spin-orbit splitting in the valence bands. The control of the spin transport properties with an in-plane electric field is the next challenge for future possible applications in spin(valley)tronics.

We thank I. Paradeisanos, F. Cadiz, T. Amand and H. Dery for useful discussions. This work was supported by the French Agence Nationale de la Recherche under the program ESR/EquipEx+(grant number ANR-21-ESRE-0025) and the ANR projects ATOEMS, Sizmo-2D and Magicvalley. This study has been partially supported through the EUR grant NanoX No. ANR-17-EURE-0009 in the framework of the "Programme des Investissements d'Avenir" and the Région Occitanie. The NHMFL is supported by the National Science Foundation DMR-1644779, the State of Florida, and the U.S. Department of Energy.

*These authors contributed equally to this work.
†Corresponding author.
cerobert@insa-toulouse.fr
‡Corresponding author.
xavier.marie@insa-toulouse.fr

[1] D. Xiao, G.-B. Liu, W. Feng, X. Xu, and W. Yao, Coupled Spin and Valley Physics in Monolayers of MoS_2 and Other Group-VI Dichalcogenides, Phys. Rev. Lett. **108**, 196802 (2012).

[2] G. Sallen, L. Bouet, X. Marie, G. Wang, C. R. Zhu, W. P. Han, Y. Lu, P. H. Tan, T. Amand, B. L. Liu, and B. Urbaszek, Robust optical emission polarization in MoS_2 monolayers through selective valley excitation, Phys. Rev. B **86**, 081301 (2012).

[3] K. F. Mak, K. He, J. Shan, and T. F. Heinz, Control of valley polarization in monolayer MoS_2 by optical helicity, Nat. Nanotechnol. **7**, 494 (2012).

[4] T. Cao, G. Wang, W. Han, H. Ye, C. Zhu, J. Shi, Q. Niu, P. Tan, E. Wang, B. Liu, and J. Feng, Valley-selective circular dichroism of monolayer molybdenum disulphide, Nat. Commun. **3**, 887 (2012).

[5] P. Dey, L. Yang, C. Robert, G. Wang, B. Urbaszek, X. Marie, and S. A. Crooker, Gate-Controlled Spin-Valley Locking of Resident Carriers in WSe_2 Monolayers, Phys. Rev. Lett. **119**, 137401 (2017).

[6] J. Li, M. Goryca, K. Yumigeta, H. Li, S. Tongay, and S. A. Crooker, Valley relaxation of resident electrons and holes in a monolayer semiconductor: Dependence on carrier density and the role of substrate-induced disorder, Phys. Rev. Mater. **5**, 044001 (2021).

[7] J. Kim *et al.*, Observation of ultralong valley lifetime in WSe_2/MoS_2 heterostructures, Sci. Adv. **3**, e1700518 (2017).

[8] L. Wang and M. W. Wu, Electron spin diffusion in monolayer MoS_2, Phys. Rev. B **89**, 205401 (2014).

[9] X. Lin, W. Yang, K. L. Wang, and W. Zhao, Two-Dimensional Spintronics for Low-Power Electronics Nat. Electron. **2**, 274 (2019).

[10] P. Back, M. Sidler, O. Cotlet, A. Srivastava, N. Takemura, M. Kroner, and A. Imamoğlu, Giant Paramagnetism-Induced Valley Polarization of Electrons in Charge-Tunable Monolayer $MoSe_2$, Phys. Rev. Lett. **118**, 237404 (2017).

[11] M. E. Flatté and J. M. Byers, Spin Diffusion in Semiconductors, Phys. Rev. Lett. **84**, 4220 (2000).

[12] J. E. H. Braz, B. Amorim, and E. V. Castro, Valley-polarized magnetic state in hole-doped monolayers of transition-metal dichalcogenides, Phys. Rev. B **98**, 161406 (2018).

[13] D. K. Mukherjee, A. Kundu, and H. A. Fertig, Spin response and collective modes in simple metal dichalcogenides, Phys. Rev. B **98**, 184413 (2018).

[14] J. G. Roch, Dmitry Miserev, G. Froehlicher, N. Leisgang, L. Sponfeldner, K. Watanabe, T. Taniguchi, J. Klinovaja, D. Loss, and R. J. Warburton, First-Order Magnetic Phase Transition of Mobile Electrons in Monolayer MoS_2, Phys. Rev. Lett. **124**, 187602 (2020).

[15] T. S. Ghiasi, J. Ingla-Aynés, A. A. Kaverzin, and B. J. van Wees, Large proximity-induced spin lifetime anisotropy in transition-metal dichalcogenide/graphene heterostructures, Nano Lett. **17**, 7528 (2017).

[16] Y. K. Luo, J. Xu, T. Zhu, G. Wu, E. J. McCormick, W. Zhan, M. R. Neupane, and R. K. Kawakami, Opto-valleytronic spin injection in monolayer MoS2/few-layer graphene hybrid spin valves, Nano Lett. **17**, 3877 (2017).
[17] M. Schwemmer, P. Nagler, A. Hanninger, C. Schüller, and T. Korn, Long-lived spin polarization in n-doped $MoSe_2$ monolayers, Appl. Phys. Lett. **111**, 082404 (2017).
[18] E. J. McCormick, M. J. Newburger, Y. K. Luo, K. M. McCreary, S. Singh, I. B. Martin, E. J. Cichewicz, B. T. Jonker, and R. K. Kawakami, Imaging spin dynamics in monolayer WS_2 by time-resolved Kerr rotation microscopy, 2D Mater. **5**, 011010 (2017).
[19] M. Kulig, J. Zipfel, P. Nagler, S. Blanter, C. Schüller, T. Korn, N. Paradiso, M. M. Glazov, and A. Chernikov, Exciton Diffusion and Halo Effects in Monolayer Semiconductors, Phys. Rev. Lett. **120**, 207401 (2018).
[20] G. Wang, A. Chernikov, M. M. Glazov, T. F. Heinz, X. Marie, T. Amand, and B. Urbaszek, Colloquium: Excitons in atomically thin transition metal dichalcogenides, Rev. Mod. Phys. **90**, 021001 (2018).
[21] F. Cadiz *et al.*, Exciton diffusion in WSe_2 monolayers embedded in a van Der Waals heterostructure, Appl. Phys. Lett. **112**, 152106 (2018).
[22] D. Unuchek, A. Ciarrocchi, A. Avsar, K. Watanabe, T. Taniguchi, and A. Kis, Room-temperature electrical control of exciton flux in a van Der Waals heterostructure, Nature (London) **560**, 340 (2018).
[23] R. Perea-Causín, S. Brem, R. Rosati, R. Jago, M. Kulig, J. D. Ziegler, J. Zipfel, A. Chernikov, and E. Malic, Exciton propagation and halo formation in two-dimensional materials, Nano Lett. **19**, 7317 (2019).
[24] T. Hotta, S. Higuchi, A. Ueda, K. Shinokita, Y. Miyauchi, K. Matsuda, K. Ueno, T. Taniguchi, K. Watanabe, and R. Kitaura, Exciton diffusion in *h*BN-encapsulated monolayer $Mose_2$, Phys. Rev. B **102**, 115424 (2020).
[25] S. Batalden and V. Sih, Spatially-resolved measurements of spin valley polarization in MOCVD-grown monolayer WSe_2, Opt. Express **29**, 17269 (2021).
[26] E. Barré, J. A. C. Incorvia, S. H. Kim, C. J. McClellan, E. Pop, H.-S. P. Wong, and T. F. Heinz, Spatial separation of carrier spin by the valley Hall effect in monolayer WSe_2 transistors, Nano Lett. **19**, 770 (2019).
[27] S. Liang *et al.*, Electrical spin injection and detection in molybdenum disulfide multilayer channel, Nat. Commun. **8**, 14947 (2017).
[28] C. Jin *et al.*, Imaging of pure spin-valley diffusion current in WS_2-WSe_2 heterostructures, Science **360**, 893 (2018).
[29] C. Robert *et al.*, Measurement of Conduction and Valence Bands g -Factors in a Transition Metal Dichalcogenide Monolayer, Phys. Rev. Lett. **126**, 067403 (2021).
[30] See Supplemental Material at http://link.aps.org/supplemental/10.1103/PhysRevLett.129.027402 for details on sample fabrication, experimental setup and dependences of the spin polarization with pump and probe power and doping density.
[31] F. Cadiz *et al.*, Excitonic Linewidth Approaching the Homogeneous Limit in MoS_2-Based van Der Waals Heterostructures, Phys. Rev. X **7**, 021026 (2017).
[32] A. Castellanos-Gomez, M. Buscema, R. Molenaar, V. Singh, L. Janssen, H. S. J. van der Zant, and G. A. Steele, Deterministic transfer of two-dimensional materials by all-dry viscoelastic stamping, 2D Mater. **1**, 011002 (2014).
[33] Z. Wang, J. Shan, and K. F. Mak, Valley- and spin-polarized Landau levels in monolayer WSe_2, Nat. Nanotechnol. **12**, 144 (2017).
[34] E. Liu, J. van Baren, T. Taniguchi, K. Watanabe, Y.-C. Chang, and C. H. Lui, Landau-Quantized Excitonic Absorption and Luminescence in a Monolayer Valley Semiconductor, Phys. Rev. Lett. **124**, 097401 (2020).
[35] A. M. Jones, H. Yu, J. R. Schaibley, J. Yan, D. G. Mandrus, T. Taniguchi, K. Watanabe, H. Dery, W. Yao, and X. Xu, Excitonic luminescence upconversion in a two-dimensional semiconductor, Nat. Phys. **12**, 323 (2016).
[36] E. Courtade *et al.*, Charged excitons in monolayer WSe_2: Experiment and theory, Phys. Rev. B **96**, 085302 (2017).
[37] M. He *et al.*, Valley phonons and exciton complexes in a monolayer semiconductor, Nat. Commun. **11**, 618 (2020).
[38] M. M. Glazov, Optical properties of charged excitons in two-dimensional semiconductors, J. Chem. Phys. **153**, 034703 (2020).
[39] C. Robert *et al.*, Spin/valley pumping of resident electrons in WSe_2 and WS_2 monolayers, Nat. Commun. **12**, 5455 (2021).
[40] M. T. Portella-Oberli, J. Berney, L. Kappei, F. Morier-Genoud, J. Szczytko, and B. Deveaud-Plédran, Dynamics of Trion Formation in In_xGa_xAs Quantum Wells, Phys. Rev. Lett. **102**, 096402 (2009).
[41] J. M. Kikkawa and D. D. Awschalom, Lateral drag of spin coherence in gallium arsenide, Nature (London) **397**, 139 (1999).
[42] S. A. Crooker and D. L. Smith, Imaging Spin Flows in Semiconductors Subject to Electric, Magnetic, and Strain Fields, Phys. Rev. Lett. **94**, 236601 (2005).
[43] J. Zipfel, K. Wagner, J. D. Ziegler, T. Taniguchi, K. Watanabe, M. A. Semina, and A. Chernikov, Light–matter coupling and non-equilibrium dynamics of exchange-split trions in monolayer WS_2, J. Chem. Phys. **153**, 034706 (2020).
[44] R. Pisoni *et al.*, Interactions and Magnetotransport through Spin-Valley Coupled Landau Levels in Monolayer MoS_2, Phys. Rev. Lett. **121**, 247701 (2018).
[45] S. Larentis, H. C. P. Movva, B. Fallahazad, K. Kim, A. Behroozi, T. Taniguchi, K. Watanabe, S. K. Banerjee, and E. Tutuc, Large effective mass and interaction-enhanced Zeeman splitting of *K*-valley electrons in $MoSe_2$, Phys. Rev. B **97**, 201407 (2018).
[46] Y. Wang, T. Sohier, K. Watanabe, T. Taniguchi, M. J. Verstraete, and E. Tutuc, Electron mobility in monolayer WS_2 encapsulated in hexagonal boron-nitride, Appl. Phys. Lett. **118**, 102105 (2021).
[47] T. Sasaki, T. Oikawa, T. Suzuki, M. Shiraishi, Y. Suzuki, and K. Noguchi, Temperature dependence of spin diffusion length in silicon by Hanle-type spin precession, Appl. Phys. Lett. **96**, 122101 (2010).
[48] N. P. Stern, D. W. Steuerman, S. Mack, A. C. Gossard, and D. D. Awschalom, Drift and diffusion of spins generated by the spin Hall effect, Appl. Phys. Lett. **91**, 062109 (2007).

[49] M. Furis, D. L. Smith, S. Kos, E. S. Garlid, K. S. M. Reddy, C. J. Palmstrøm, P. A. Crowell, and S. A. Crooker, Local Hanle-effect studies of spin drift and diffusion in n:GaAs epilayers and spin-transport devices, New J. Phys. **9**, 347 (2007).

[50] S. G. Carter, Z. Chen, and S. T. Cundiff, Optical Measurement and Control of Spin Diffusion in *n*-Doped GaAs Quantum Wells, Phys. Rev. Lett. **97**, 136602 (2006).

[51] C. Hu, H. Ye, G. Wang, H. Tian, W. Wang, W. Wang, B. Liu, and X. Marie, Room temperature spin diffusion in (110) GaAs/AlGaAs quantum wells, Nanoscale Res. Lett. **6**, 149 (2011).

[52] G. Wang, B. L. Liu, A. Balocchi, P. Renucci, C. R. Zhu, T. Amand, C. Fontaine, and X. Marie, Gate control of the electron spin-diffusion length in semiconductor quantum wells, Nat. Commun. **4**, 2372 (2013).

[53] N. Tombros, C. Jozsa, M. Popinciuc, H. T. Jonkman, and B. J. van Wees, Electronic spin transport and spin precession in single graphene layers at room temperature, Nature (London) **448**, 571 (2007).

[54] M. Drögeler, C. Franzen, F. Volmer, T. Pohlmann, L. Banszerus, M. Wolter, K. Watanabe, T. Taniguchi, C. Stampfer, and B. Beschoten, Spin lifetimes exceeding 12 Ns in graphene nonlocal spin valve devices, Nano Lett. **16**, 3533 (2016).

[55] K. Hao, R. Shreiner, and A. A. High, Optically controllable magnetism in atomically thin semiconductors, arXiv:2108.05931.

[56] D. Edelberg *et al.*, Approaching the intrinsic limit in transition metal diselenides via point defect control, Nano Lett. **19**, 4371 (2019).